The Cryosphere, 12, 3177–3186, 2018
https://doi.org/10.5194/tc-12-3177-2018

The Cryosphere Open Access EGU

Iron oxides in the cryoconite of glaciers on the Tibetan Plateau: abundance, speciation and implications

Zhiyuan Cong[1,5], Shaopeng Gao[1], Wancang Zhao[3], Xin Wang[4], Guangming Wu[1,6], Yulan Zhang[2], Shichang Kang[2,5], Yongqin Liu[1], and Junfeng Ji[3]

[1]Key Laboratory of Tibetan Environment Changes and Land Surface Processes, Institute of Tibetan Plateau Research, Chinese Academy of Sciences, Beijing 100101, China
[2]State Key Laboratory of Cryospheric Sciences, Northwest Institute of Eco-Environment and Resources, Chinese Academy of Sciences, Lanzhou 730000, China
[3]Key Laboratory of Surficial Geochemistry, Ministry of Education, School of Earth Sciences and Engineering, Nanjing University, Nanjing 210023, China
[4]Key Laboratory for Semi-Arid Climate Change of the Ministry of Education, College of Atmospheric Sciences, Lanzhou University, Lanzhou 730000, China
[5]CAS Center for Excellence in Tibetan Plateau Earth Sciences, Beijing 100101, China
[6]University of Chinese Academy of Sciences, Beijing 100049, China

Correspondence: Shichang Kang (shichang.kang@lzb.ac.cn)

Received: 6 April 2018 – Discussion started: 25 May 2018
Revised: 23 August 2018 – Accepted: 6 September 2018 – Published: 5 October 2018

Abstract. Cryoconite is a mixture of impurities and ice visually represented by dark colors present in the ablation zone of glaciers. As an important constituent of light-absorbing impurities on the glacier surface, iron oxides influence the radiative properties of mineral dust and thus its impact on ice melting processes. In particular, the distinct optical properties between hematite and goethite (the major iron oxide species) highlight the necessity to obtain accurate knowledge about their abundance and geochemical behavior. Cryoconite samples from five glaciers in different regions of the Tibetan Plateau (TP) and surroundings were studied. The iron abundance in the cryoconite from TP glaciers ranged from 3.40 % to 4.90 % by mass, in accordance with typical natural background levels. Because the light absorption capacity of mineral dust essentially depends on the presence of iron oxides (i.e., free iron), iron oxides were extracted and determined using diffuse reflectance spectroscopy. The ratios of free to total iron for the five glaciers ranged from 0.31 to 0.70, emphasizing that iron in the form of oxides should be considered rather than total iron in the albedo and radiative modeling. Furthermore, the goethite content in iron oxides (in mass fraction) ranged from 81 % to 98 %, showing that goethite was the predominant form among the glaciers. Using the abundance and speciation of iron oxides as well as their optical properties, the total light absorption was quantitatively attributed to goethite, hematite, black carbon (BC) and organic matters at 450 and 600 nm wavelengths. We found that the goethite played a stronger role than BC at shorter wavelengths for most glaciers. Such findings were essential to understand the relative significance of anthropogenic and natural effects, and then taking the proper mitigation measures.

1 Introduction

The light-absorbing impurities (LAIs) in glaciers can significantly reduce the surface albedo of snowpack and absorb more solar energy (Warren and Wiscombe, 1985). LAIs were recognized as a major contributor to glacier and ice sheet melting (Qian et al., 2015, and references therein), along with rising air temperatures (IPCC, 2014). The composition of LAIs on the glacier surface is very complex. Their major constituents include BC, brown carbon, mineral dust and biogenic matter (Baccolo et al., 2017; Kaspari et al., 2015; Pu et al., 2017; Takeuchi, 2002). The composition of LAIs is particularly complex when considering mountain glaciers from

the Himalayas and Tibetan Plateau (TP) (Fig. 1). In summer, their surfaces are commonly covered by incoherent impurities (granular sediment) with a dark color, which was termed cryoconite (Baccolo et al., 2017; Dong et al., 2016).

Presently, tremendous attention has been paid to the BC in glaciers (Kaspari et al., 2011; Wang et al., 2015; Yasunari et al., 2010) because the glaciated areas of the TP are in the vicinity of intensive BC source regions, e.g., South Asia (Cong et al., 2015). In contrast, little research has focused on dust in this region despite dust apparently being the predominant constituent of impurities on the glacier surface, especially in its ablation area (Qian et al., 2015). Based on field research at Mera Glacier in the Nepalese Himalayas, Kaspari et al. (2014) pointed out that when dust loading is high, the snow albedo reduction and subsequent radiative forcing caused by dust will overwhelm the impact related to BC.

To quantify the relative contribution of dust and BC as well as other substances is challenging (Painter et al., 2010). In the snow albedo simulation models like SNICAR (Flanner and Zender, 2006), dust concentration (micrograms of dust per gram of ice) was employed to represent the loading of dust, without considering the dust composition. Actually, the light absorption capacity of dust essentially depends on the presence of iron oxides (also commonly termed "free iron") (Alfaro et al., 2004; Formenti et al., 2014; Moosmüller et al., 2012; Shi et al., 2012). The most common iron oxide species in mineral dust are hematite (Fe_2O_3) and goethite (FeO(OH)), which have distinct optical properties in terms of absorption and wavelength dependence (Balsam et al., 2014). At the same time, some parts of iron are incorporated into the crystal lattice of alumino-silicates (defined as structural iron), and they do not contribute to the absorption of solar light (Lafon et al., 2006).

Up to now, the iron abundance and especially its mineral phases in glacial areas were not well understood (Hawkings et al., 2018; Shahgedanova et al., 2013). The degree to which iron oxides contribute to solar absorption and reduction of snow albedo remains uncertain. To constrain the uncertainties of estimating the radiative forcing of cryoconite, particularly in the TP glacier area, we designed this research to address several key issues. What is the abundance of iron in the cryoconite of mountain glaciers? What fraction of the total iron exists as iron oxides with efficient light absorption capability? What is the relative proportion of hematite and goethite, considering their distinct optical characteristics? What is their spatial variation in different types of glacier? Furthermore, how do the iron oxides impact the absorbing properties of cryoconite?

Figure 1. Surface of mountain glacier **(a)** in the central Tibetan Plateau and dispersed cryoconite **(b)** on it.

2 Field sampling and laboratory measurements

2.1 Field sampling

In order to consider geographic variability, five glaciers in different regions of TP and surroundings were chosen for the cryoconite sampling (Fig. 2). A detailed description of the collection sites is given in Table 1. The Urumqi no. 1 Glacier (hereafter donated as UG, 43°06′ N, 86°49′ E) presents two branches covering 1.646 km^2. It is located in the eastern Tien Shan. The air circulation regime there is dominated by the westerlies in summer and by the influence of the Siberian High during winter (Wang et al., 2014). Laohugou Glacier (LHG, 39°28′ N, 96°32′ E), with a length of 10 km and an area of 20 km^2, is at the northern slope of the western Qilian Mountains with typical continental climatic conditions (Dong et al., 2014). That area is surrounded by large sandy deserts in northwest China, like Taklimakan Desert to the west, Qaidam Basin to the southwest and the Gobi Desert to the north. Xiaodongkemadi Glacier (XDK,

Table 1. Summary of cryoconite samples collected from five glaciers over the Tibetan Plateau and surroundings.

Glacier	Description	Coordinates	Elevation (m a.s.l.)	Sampling date	Sample number
Urumqi no. 1 Glacier (UG)	Tien Shan	43°06′ N, 86°48′ E	3800–4000	August 2014	14
Laohugou (LHG)	Qilian Mount.	39°28′ N, 96°32′ E	4300–4900	July 2014	14
Xiaodongkemadi (XDK)	Tanggula Mount.	33°03′ N, 92°04′ E	5400–5600	August 2014	6
Palong no. 4 (PL)	Southeast TP	29°15′ N, 96°56′ E	4700	September 2015	2
Baishui no. 1 Glacier (BS)	Yulong	27°6′ N, 100°11′ E	4600–4800	August 2014	9

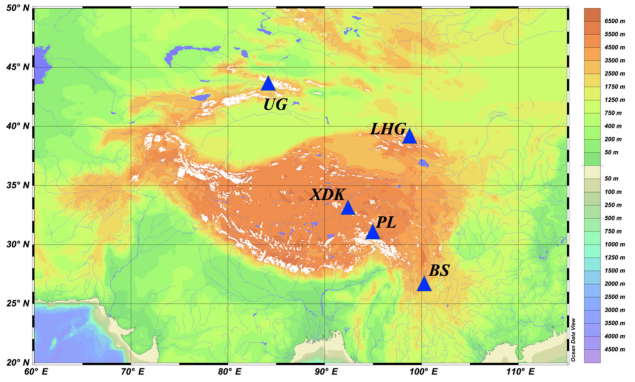

Figure 2. Topographic map of the Tibetan Plateau and surroundings, with locations of the five representative glaciers. The base map was created using Ocean Data View software (Schlitzer, 2017).

33°03′ N, 92°04′ E) is located on the northern slope of the Tanggula Mountains, at the center of the TP. Previous studies showed that the Tanggula Mountains represent the northern boundary of the area influenced by the South Asian monsoon (Tian et al., 2001). Palong no. 4 Glacier (PL, 29°15′ N, 96°56′ E), located in the southeast TP, is a typical temperate glacier. It is strongly influenced by the South Asian summer monsoon intruding via the Brahmaputra Valley, and it is characterized by high accumulation (2500–3000 mm) and ablation rates on an annual scale (Yang et al., 2016). Baishui no. 1 Glacier (BS, 27°6′ N, 100°11′ E), with a length of 2.26 km and an area of 1.32 km^2, is the largest glacier in the Yulong Mountains, at the southeastern edge of the TP. It is characterized by high precipitation, a low snow line and relatively high temperatures (equilibrium line mean annual value of −6 °C, summer value of 1–5 °C) (Niu et al., 2013).

Cryoconite samples were collected using a stainless-steel scoop on the surfaces of five glaciers described above. Samples were preserved in Nalgene HDPE wide-mouth bottles (500 mL) and kept frozen until analysis. In the laboratory, the cryoconite samples were freeze-dried into powder. In this work, concentrations and fractions are referred to as dry cryoconite mass. Therefore, our measurements mainly reflect processes occurring in summer on the glacier surface.

2.2 Elemental analysis by ICP-MS

A portion of cryoconite sample (about 20 mg) was dissolved under a laboratory hood using a HF + HNO_3 mixture through three steps. In detail, the sample was first transferred into a PTFE high-pressure digestion vessel, and 1 mL of HF and 1 mL of HNO_3 were added. The digestion vessel was then ultrasonically treated for 20 min and evaporated to nearly dry on a hot plate. Another 1 mL of HF and 1 mL of HNO_3 were added and digested in an oven at 190 °C for 24 h. After cooling, the vessel was opened and evaporated to nearly dry again (on the plate at 150 °C), followed by a second addition of HNO_3. This procedure was repeated to remove HF completely. Then 1 mL of HNO_3 and 3 mL of H_2O were added to the vessel, which was placed into the oven for another 24 h at 150 °C. After cooling, the final solution was diluted with pure water to about 50 mL.

After treatment, each sample was measured using inductively coupled plasma mass spectrometry (ICP-MS, Thermo X7, Thermo-Elemental Corp.) for Fe and other elements. Indium, rhodium and rhenium solutions were used as internal standards. The accuracy and precision of trace elements was ascertained based on repeated measurement of the USGS geochemical reference standard (Andesite, AGV-2). The measured and certified values for Fe agree well, with recovery of better than 95 %. The detailed description of the analytical protocol in our laboratory can be found in previous work (Wu et al., 2009).

2.3 Total organic carbon and black carbon

The contents of organic carbon were determined by a total organic carbon (TOC) analyzer (TOC-V, Shimadzu). The accuracy of the TOC analysis was ±5 %. The separation and analysis of BC in the cryoconite were adopted from procedures previously developed for sediments (Cong et al., 2013; Han et al., 2011). Specifically, the samples were first freeze-dried, then ground into powder and weighed. Then, HCl (2N) was added to remove carbonates, silicates and some kinds of metal oxides. The solution was centrifuged to remove the supernatants. Then a mixture (1 : 2) of HCl (6N) and HF (48 %) was added into the residue and reacted further. Finally, the residual solid was diluted with ultrapure water and filtered using a quartz fiber filter with even distribution on the sur-

face (QM-A grade; Whatman International Ltd., England). The quartz filters were analyzed for BC using a DRI model 2001 carbon analyzer. For quality control, standard reference material (marine sediment, NIST SRM-1941b) was also analyzed (Cong et al., 2013). Our BC values compare well to the value reported by Han et al. (2007) (> 95 %, $n = 5$), which indicates the analytical method used is reliable and repeatable.

2.4 Extraction and quantification of iron oxides

Cryoconite samples were treated with the citrate–bicarbonate–dithionite (CBD) method three times to completely extract iron oxides (Ji et al., 2002; Lafon et al., 2004; Mehra and Jackson, 1958). Then dissolved Fe^{3+} concentrations in the CBD solution were determined using a UV-2100 spectrophotometer (Unico Inc., Shanghai) to obtain the iron mass in the form of oxides, Fe(ox), relevant to the light absorption in the visible light. Uncertainties for the Fe(ox) analysis were less than 5 %. The remaining iron, i.e., the structural iron, was calculated by subtracting the Fe(ox) from total iron.

$$\mathrm{Fe(struc)} = \mathrm{Fe(tot)} - \mathrm{Fe(ox)}$$

Here CFe(tot) is the total iron concentration achieved from ICP-MS elemental analysis.

2.5 Hematite–goethite measurement using diffuse reflectance spectroscopy

Given the low abundance of Fe in the cryoconite, the speciation of iron oxides cannot be achieved by traditional mineralogical analysis methods like X-ray diffraction (XRD). In this study, diffuse reflectance spectroscopy (DRS) was employed to distinguish and quantify hematite and goethite. Measurements were conducted using a Perkin-Elmer LAMBDA 900 spectrophotometer (Perkin-Elmer Corp., Norwalk, CT) equipped with a diffuse reflectance attachment. Analyses were performed for spectra in the range from 400 to 700 nm with an interval of 2 nm. Detailed procedures have been described well previously (Ji et al., 2002; Lu et al., 2017). Hematite and goethite are the two main coloring agents in mineral dusts and are characterized by distinct colors, red and yellow, respectively. Hematite was chosen to be quantified rather than goethite because hematite is a more intense (effective) coloring agent than goethite. The limit of detection for Hm can be as low as 0.01 % by weight (Balsam et al., 2014; Deaton and Balsam, 1991; Ji et al., 2002; Lu et al., 2017).

A set of calibration samples containing known hematite were measured. Then the percent reflectance in the red color band (630–700 nm, redness) was used as an independent variable in a transfer function for calculating hematite, which was established through a regression as follows:

$$\mathrm{Hm(wt\,\%)} = 1 \times 10^6 \times e^{27.37 \cdot \mathrm{Redness}}$$
$$\left(R^2_{\mathrm{adj}} = 0.9301,\ \ \mathrm{RMSE} = 0.3018\right).$$

Assuming the CBD-extracted Fe (in the form of iron oxides) is only constituted by hematite (Hm) and goethite (Gt), the content of goethite could be calculated using the following equation:

$$\mathrm{Gt(wt\,\%)} = 1.59 \times \left(\mathrm{Fe_{(ox)}} - \mathrm{Hm}/1.43\right).$$

The reproducibility standard deviation of reflectance at all wavelengths was less than 0.15 % (Lu et al., 2017).

2.6 Light absorption of cryoconite

Measurements of light absorption were performed using an ISSW spectrophotometer in Lanzhou University, China. The experimental strategy was mainly based on the method described by Doherty et al. (2010) and Wang et al. (2013). The ISSW measurement system is specially designed to be sensitive to light absorption and to avoid the interference of light scattering (Grenfell et al., 2011). The ISSW spectrophotometer could provide the spectral absorption properties of cryoconite, by weighting the transmitted light (I) for a sample and that for a blank filter (I_0). The relative attenuation (x_λ) is described by the natural logarithm of I_0/I:

$$x_\lambda = \ln\left[I_0(\lambda) I(\lambda)\right]. \quad (1)$$

The spectrum of light attenuation was further calibrated by a set of BC standards (fullerene soot, Alfa Aesar Inc., Ward Hill, MA, USA) (Fig. S1 in the Supplement). Because the ISSW spectrophotometer is only sensitive to the signal of light absorption but not scattering of LAIs on filters due to its integrating sandwich structure, the light attenuation by samples on the filter at specific wavelengths will be converted to equivalent BC mass loading (L_{BC}, $\mu\mathrm{g\,C\,cm^{-2}}$), which allows us to calculate absorption optical depth $\tau(\lambda)$ by cryoconite: $\tau_\lambda = L_{\mathrm{BC}}\beta_\lambda$. Here β_λ is the mass absorption coefficient (MAC) of standard BC (i.e., fullerene, $6.3\,\mathrm{m^2\,g^{-1}}$ at 550 nm) (Grenfell et al., 2011; Zhou et al., 2017). Then the light absorption capacity of cryoconite was calculated by dividing the absorption optical depth by the mass loading on the filter:

$$\mathrm{MAC} = \tau_\lambda / L. \quad (2)$$

The absorption Ångström exponent (AAE) describes the wavelength dependence of the light absorption by particles (Ångström, 1929). The value of AAE could be obtained using the formula $\mathrm{AAE} = -\ln(\tau_1/\tau_2)/\ln(\lambda_1/\lambda_2)$, where τ_1 and τ_2 are the light attenuation calculated at the given wavelengths λ_1 and λ_2, respectively. The standard deviation between repeated measurements ranges from 0.29 % to 7.83 % (mean value: 2.92 %).

Table 2. The abundances (by mass) of total iron, free iron, hematite, goethite and their ratios determined in cryoconites from TP glaciers, as well as other data available in the literature.

Locations	Description	Total iron (%)	Free iron (%)	Free / total iron ratio	Hematite (%)	Goethite (%)	Gt / Hm ratio	References
UG		4.62 (±0.22)[a]	1.41 (±0.29)	0.31 (±0.07)	0.24 (±0.02)	1.98 (±0.47)	8.26 (±2.27)	This study
LHG		4.28 (±0.17)	1.50 (±0.30)	0.35 (±0.07)	0.28 (±0.02)	2.08 (±0.48)	7.54 (±1.83)	This study
XDK	Cryoconite	3.40 (±0.18)	1.93 (±0.48)	0.56 (±0.12)	0.56 (±0.08)	2.44 (±0.69)	4.30 (±0.90)	This study
PL		4.18 (±0.13)	1.53 (±0.28)	0.37 (±0.08)	0.23 (±0.01)	2.18 (±0.44)	9.63 (±1.88)	This study
BS		4.90 (±0.21)	3.43 (±0.53)	0.70 (±0.10)	0.10 (±0.01)	5.35 (±0.85)	55.2 (±10.4)	This study
Swiss Alps	Cryoconite	4.0 (±0.7)						Baccolo et al. (2017)
Utah, USA	Dust on snow	1.73–2.85					∼ 1[b]	Reynolds et al. (2014)
Niger, Sahara	Desert aerosol	6.3 (±0.9)	2.8 (±0.8)	0.44 (±0.11)				Lafon et al. (2004)
Niger, Sahel	Desert aerosol	7.8 (±0.4)	5.0 (±0.4)	0.65 (±0.04)				Lafon et al. (2004)
Yulin, China	Desert aerosol	7.7 (±0.3)	3.7 (±0.4)	0.48 (±0.03)				Lafon et al. (2004)
ZBT, China	Desert aerosol	5.38 (±0.2)	3.0 (±0.2)	0.43 (±0.01)			∼ 3.0	Lafon et al. (2006)
West Africa	Desert aerosol			0.38–0.72	0.09–0.26[c]	0.21–0.49[c]	0.96–3.1	Formenti et al. (2014)

[a] Values in brackets represent the standard deviations.
[b] Mössbauer spectroscopy indicated roughly equal amounts of hematite and goethite, while reflectance spectroscopy showed goethite was dominant in iron oxides.
[c] Using X-ray absorption (XAS). Note that the total and free iron data in this table were obtained using ICP-MS so they refer to the elemental Fe, while hematite and goethite were measured as Fe oxides.

3 Results and discussion

3.1 Organic carbon and black carbon contents

The total organic carbon and BC mass fractions of the cryoconite from the five glaciers are presented in Fig. 3. The most striking feature was that BS exhibited the highest TOC content (9.70 ± 0.99 % in mass faction), about 4 times higher than the other four glaciers. Similarly, the BC in the cryoconite from BS was also significantly higher than other glaciers, i.e., UG, LHG, XDK and PL. For the BC concentration, BS also has the highest abundance (1.99 ± 0.28 % in mass), indicating the strong anthropogenic (fossil fuel and biomass burning) influence there. For the remaining four glaciers, their BC contents were comparable, ranging from 0.06 ± 0.01 % (in total mass of dried cryoconite) at XDK to 0.13 ± 0.03 % at PL. For comparison, Di Mauro et al. (2017) reported the BC values in cryoconites from Morteratsch Glacier (Swiss Alps) in the range of 0.30–0.4 % in mass faction.

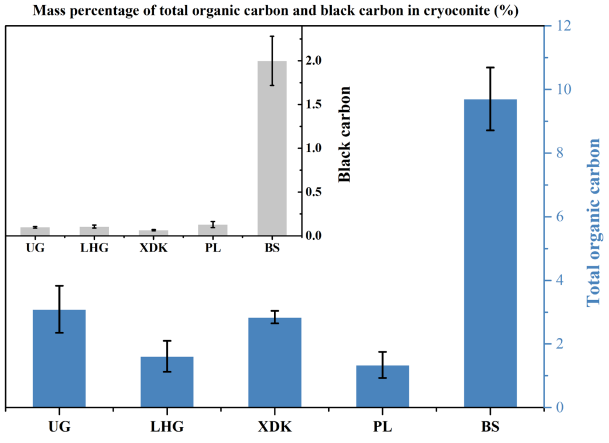

Figure 3. The total organic carbon (blue) and black carbon (grey) in the total mass of cryoconites on the mountain glaciers of the Tibetan Plateau and surroundings.

3.2 Abundance of elemental Fe (total) and free Fe (iron oxides)

The iron contents found in cryoconite samples from UG, LHG, XDK, PL and BS averaged 4.62 %, 4.28 %, 3.40 %, 4.18 % and 4.90 %, by mass, respectively (Fig. 4). Our data were similar to the previous reported iron contents in dust particles preserved in ice cores across the TP (Wu et al., 2012), which ranged from 3.38 % to 5.41 %. The iron in the cryoconite on the TP glaciers represents a natural background level. Lower iron contents were found in the dust layers deposited on snow cover in northern Utah, USA (the Wasatch Range), which varied from 1.73 % to 2.85 % by mass (Reynolds et al., 2014). Given the scarce information of Fe abundance available in the glacier area, we also briefly summarized the data in mineral dust from various desert regions worldwide for comparison (Table 2). The determined Fe contents in desert aerosols from ZBT (Zhengbeitai) and Yulin in north China were 5.38 % and 7.7 % in total dust aerosol mass, respectively, somewhat higher than our values of cryoconite over glaciers. The reported values of Fe content from the Sahara and Arabian Peninsula generally varied in the range from 2.0 % to 11 % by mass (Gao et al., 2001; Gomes and Gillette, 1993; Zhang et al., 2015), depending on the locations and the transport process. Recently, Caponi et al. (2017) reported the mass fraction of Fe in global dust aerosols ($PM_{10.6}$) ranged from 2.8 % (Namibia) to 7.3 % (Australia). In addition, in this study there was no systematic

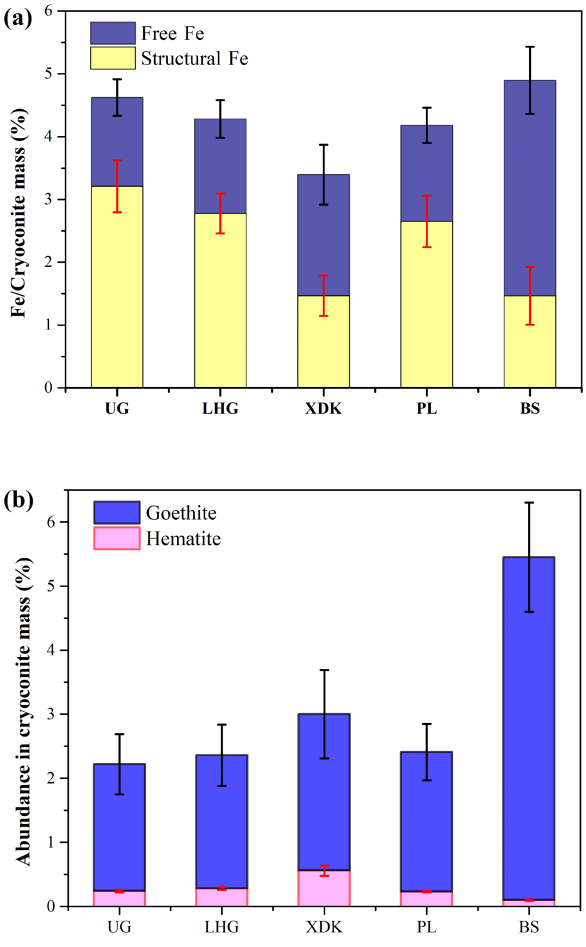

Figure 4. The free iron and structural iron contents (elemental Fe) measured in the total cryoconite (dried) mass from TP glaciers **(a)**, and goethite and hematite (Fe oxides) contents in the total cryoconite mass **(b)**.

variation in the Fe concentrations with altitude, which indicated that the cryoconite on each glacier was a homogeneous mixture. The comparable levels of iron (3.4 %–4.9 %) found in the five glaciers in different parts of the TP demonstrated that there is little regional variability in elemental iron in the cryoconites, which is likely related to the mineralogical composition of parent soils.

Because only iron oxides (free iron) could effectively control the absorbing property of mineral materials, the content of free iron is more concerned in radiative and climate modeling. Table 2 shows the means of free and structural iron in cryoconite (percentage in total mass) from the five glaciers, with their standard deviations. Interesting, the highest value of total Fe and the highest free-to-total ratio were found in the samples from BS. The color of BS samples was darker than others visually, and they also present the highest TOC contents among the five glaciers (Fig. 3).

The ratios of free to total iron for the five glaciers ranged from 0.31 to 0.70 (Table 2). That means substantial Fe is trapped in the crystal lattice (i.e., structural Fe) and has no direct relationship with the light absorption. This finding is generally in agreement with that of Lafon et al. (2004) and Caponi et al. (2017) for desert aerosols (Table 2). Namely, only about half of total iron is in the form of iron oxides. Therefore, our result clearly demonstrates that the total iron is not suitable to be directly used in the albedo and radiative modeling, although this has been a common practice in previous research (Kaspari et al., 2014; Wang et al., 2013). If this point was considered, the contribution of iron-containing minerals to the total light absorption on the glacier surface will decrease almost 50 %; namely, the other light-absorbing components like BC and brown carbon should correspondingly account for a much larger fraction.

3.3 The speciation of iron oxides

In previous modeling studies of the dust radiative forcing, hematite was usually assumed to be the major absorbing iron oxide (Sokolik and Toon, 1999). However, in this study goethite was found to be more abundant than hematite for all five glaciers (Fig. 4 and Table 2). The goethite in total iron oxide mass ranged from 81 % (for XDK) to 98 % (for BS), showing that goethite is the predominant form of iron oxides. The ratios of goethite to hematite in our study were even higher than those reported for desert aerosols (Table 2) (Formenti et al., 2014; Lafon et al., 2006; Shen et al., 2006). For example, Lafon et al. (2004) reported the iron oxides in the dust from northwest China with about half of total iron in the form of iron oxides, and the abundance of goethite (73 % of the total iron oxide mass) was higher than hematite (27 %). Shen et al. (2006) determined comparable goethite–hematite composition data in dust aerosols from north China, i.e., 64 % for goethite in total iron oxide mass and 36 % for hematite in Dunhuang, 63 % and 37 % in Yulin, and 68 % and 32 % in Tongliao. In the dust samples collected on the snow from the western US (Wasatch Range, Utah), the amounts of goethite and hematite in dust samples were found to be roughly equal using Mössbauer spectroscopy (Reynolds et al., 2014).

In addition to the pedogenic characteristics, the dominance of goethite over hematite may be also ascribed to the glacier surface environment. Goethite formation is favored in moist and cool conditions, while hematite commonly occurs in warm and dry environments (Reynolds et al., 2014). That is also why the ratios of goethite to hematite were frequently used as indicators of paleoclimate (e.g., precipitation and temperature) (Schwertmann, 1971). Taking into account the cold and humid conditions on the glacier surface, mineralogical transformation of hematite to goethite is highly expected to happen, resulting in more goethite. Microorganisms may also play a crucial role in the degradation of rocks and minerals in terrestrial environments through changing the trans-

formation rates, pathways and even the end products (Fru et al., 2012). This is especially plausible for BS with the highest TOC content (an indicator of high microbial activity) as well as iron oxides, but more research is needed to test this hypothesis.

3.4 Contribution to light absorption by cryoconite components

Optical properties of goethite and hematite, including MAC and AAE parameters, are critical to assess their role in the light absorption. A wide range of MAC values have been reported in the literature. According to the previous work by Alfaro (2004), the MAC of iron oxides (goethite : hematite, 73 % : 27 %) in dust from northwest China desert was measured as 0.56 $m^2\,g^{-1}$ at 660 nm, and it will increase about 6 times at a shorter wavelength (325 nm) (AAE $\approx$ 3). This value was further employed to evaluate the albedo and radiative forcing effect of dust in snow of the Himalayas (Nepal) (Kaspari et al., 2014). Recently, Utry et al. (2015) reported the MAC value of hematite (purity > 95 %) as 0.54 $m^2\,g^{-1}$ at 532 nm, based on the measurements of a multi-wavelength photoacoustic instrument. Wang et al. (2013) choose a MAC of goethite of 0.9 $m^2\,g^{-1}$ (550 nm) and AAE value of 3 to assess the contribution of mineral dust to the total absorption of LAIs in north China snow. Based on the laboratory experiments by ISSW, we determined an Fe-specific absorption coefficient using the goethite (Stream Chemicals Inc.) and hematite standard (Sigma Aldrich Inc.) (Fig. 5). The calculated MAC values at 450 nm for goethite and hematite were 1.55 ± 0.08 and 1.12 ± 0.11 $m^2\,g^{-1}$, respectively. And the MAC values at 600 nm were 0.15 ± 0.01 and 0.55 ± 0.03 $m^2\,g^{-1}$, respectively. It should be noted that the MACs reported here are the values of isolated iron oxides (i.e., hematite and goethite). They are much larger than the MAC values of dust, which range from 0.013 to 0.055 $m^2\,g^{-1}$ over the world (Caponi et al., 2017).

Here we assumed that the total light absorption was entirely and exclusively caused by three components, i.e., iron oxides (goethite and hematite), BC and organic matter. Compared to dust and BC, the composition and sources of organic matter over the glacier surface are complicated. Organic matter was a mixture of soil humic and humic-like matter, biogenic particles (e.g., algae, fungi and plant debris), and biomass/fossil fuel burning emissions (Wu et al., 2016), which are often termed brown carbon (BrC). Considering its diverse sources and complex composition, in this work we did not assume the specific optical parameters for organic matter. Instead, the relative contributions to absorption by organic matter were obtained by subtracting the portions by iron oxides and BC from the total absorption. The optical properties of the latter two components are much more certain than light-absorbing organics. The mass absorption efficiency and AAE value of BC were assumed to be 6.3 $m^2\,g^{-1}$ (550 nm) and 1.1, respectively (Grenfell et al., 2011).

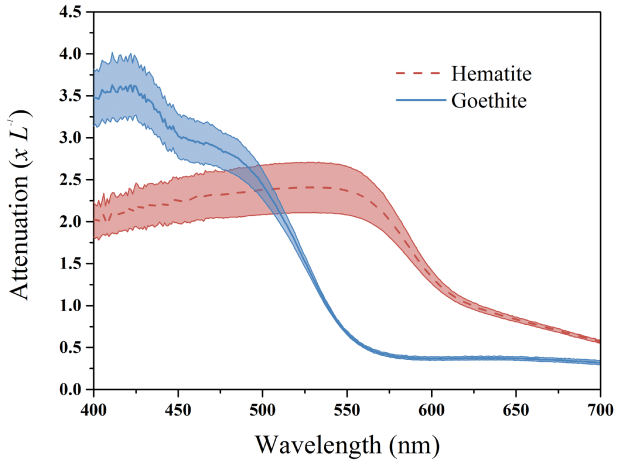

Figure 5. The mass-weighted light attenuation by hematite and goethite. Error bars indicate the standard deviation.

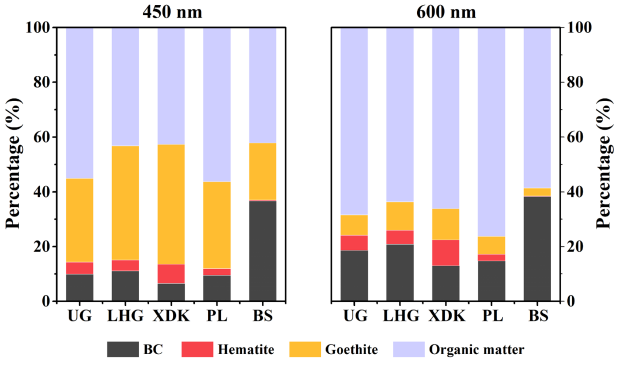

Figure 6. Apportioning of total light absorption (450 and 600 nm) to black carbon, hematite, goethite and organic matter for the cryoconite from five TP glaciers.

Because the light absorption capability of iron oxides and organic matter varies with wavelength, here we calculated the relative absorption of these three components at 450 and 600 nm, respectively. As shown in Fig. 6, at 600 nm (the right panel), organic matter dominated light absorption, and BC was the second contributor to light absorption, especially for the BS glacier with the highest BC concentration. However, the contribution of iron oxides increases dramatically at 450 nm, especially for goethite, due to their high light absorption ability at short wavelengths. For the glaciers except BS, the absorption by goethite was larger than BC and approximately equal to organic matter. The increased contribution by goethite at the shorter wavelength was due to its large AAE value (Zhou et al., 2017), which indicated stronger light absorption at short wavelengths. While the relative contribution to absorption by hematite appeared to be constant among different wavelengths.

In general, goethite plays a stronger role at a shorter band, causing a higher fraction of light absorption than BC. Although iron oxides are much less absorbing than BC per unit mass, the much higher mass concentration of mineral dust in the natural environment may result in total absorption being larger than BC.

4 Summary and conclusions

The degree to which mineral dust, especially iron oxides, affect the solar absorption and decreases in snow albedo remain uncertain. Despite their importance, the content and speciation of iron oxides in the cryoconite over the glacial surface has not been reported previously.

The iron abundances in the cryoconite from TP glaciers ranged from 3.40 % to 4.90 % by mass, which was comparable to the upper continental crust composition (3.5 % of Fe) (Taylor and McLennan, 1995) and implied natural sources. We further separated and determined iron oxides (free Fe) using the citrate–bicarbonate–dithionite method. The ratios of free to total iron for the five glaciers ranged from 0.31 to 0.70. That meant substantial amounts of Fe were trapped in the crystal lattice (i.e., structural Fe) and had no direct influence on the light absorption. Our result clearly demonstrated that the total iron was not suitable to be directly used in the albedo and radiative modeling, although this was a common practice in previous studies. The iron oxides were further quantified into goethite and hematite, the two major species. The goethite content in iron oxides (in mass fraction) ranged from 81 % (XDK) to 98 % (BS), showing that goethite was the predominant form of iron oxides. Four glaciers (i.e., UG, LHG, XDK and PL) in the main body of TP demonstrated similar patterns regarding the iron oxide abundance and speciation. However, Baishui glacier was unique in these aspects. Baishui glacier is located at the southeastern margin of TP and closely adjacent to the intensive human activities area, and it received more organic matter. The microbes in such environments may perturb the natural distribution of iron.

Taking account of both the abundance of iron oxides and their optical properties, the total light absorption was quantitatively attributed to goethite, hematite, BC and organic matter at 450 and 600 nm. Organic matter was found to be the most important light absorber at 450 and 650 nm wavelengths. We demonstrated that the goethite played a stronger role than BC at shorter wavelengths (i.e., 450 nm) for glaciers except the Baishui glacier. Although iron oxides are much less absorbing than BC per unit mass, the high mass concentration of mineral dust in the natural environment may result in total absorption larger than BC. In general, this research provided new observations of the iron oxides in glaciers, and the results are meaningful for understanding their role in mountain glacier surfaces in the Himalayas and TP, a climate-sensitive and environmentally fragile region. Currently, due to the limitation of our field sampling, we cannot obtain the spatial distribution of cryoconite on the glacier surface (i.e., the percentage of cryoconite cover in a unit area of glacier surface). In future research, we will explore quadrat sampling to reveal the exact change of albedo by cryoconite.

Data availability. The laboratory dataset is included in Table 2. Any other specific data can be provided by the authors on request.

The Supplement related to this article is available online at https://doi.org/10.5194/tc-12-3177-2018-supplement.

Author contributions. ZYC and SCK designed the study, SCK collected the field samples, and SPG, WCZ, XW, GMW, YLZ, YQL and JFJ performed laboratory measurements. All authors contributed to the discussion of the results. ZYC led the writing of the paper and all co-authors contributed to it.

Competing interests. The authors declare that they have no conflict of interest.

Acknowledgements. We deeply thank Wei Yang, Yajun Liu, Hewen Niu, Junming Guo, Zhiwen Dong, Xiaofei Li, Yang Li and other team members for their contribution in the field sampling. This work is supported by National Science Foundation of China under grants 41522103, 41522505, 41630754 and 41673095. The data used are listed in the references, tables and supplements.

Edited by: Becky Alexander
Reviewed by: two anonymous referees

References

Alfaro, S. C., Lafon, S., Rajot, J. L., Formenti, P., Gaudichet, A., and Maille, M.: Iron oxides and light absorption by pure desert dust: An experimental study, J. Geophys. Res., 109, D08208, https://doi.org/10.1029/2003JD004374, 2004.

Ångström, A.: On the atmospheric transmission of sun radiation and on dust in the air, Geografiska Annaler, 11, 156–166, 1929.

Baccolo, G., Di Mauro, B., Massabò, D., Clemenza, M., Nastasi, M., Delmonte, B., Prata, M., Prati, P., Previtali, E., and Maggi, V.: Cryoconite as a temporary sink for anthropogenic species stored in glaciers, Scientific Reports, 7, 9623, https://doi.org/10.1038/s41598-017-10220-5, 2017.

Balsam, W., Ji, J., Renock, D., Deaton, B. C., and Williams, E.: Determining hematite content from NUV/Vis/NIR spectra: Limits of detection, Am. Mineral., 99, 2280–2291, 2014.

Caponi, L., Formenti, P., Massabó, D., Di Biagio, C., Cazaunau, M., Pangui, E., Chevaillier, S., Landrot, G., Andreae, M. O., Kandler, K., Piketh, S., Saeed, T., Seibert, D., Williams, E., Balkanski, Y., Prati, P., and Doussin, J.-F.: Spectral- and size-resolved mass

absorption efficiency of mineral dust aerosols in the shortwave spectrum: a simulation chamber study, Atmos. Chem. Phys., 17, 7175–7191, https://doi.org/10.5194/acp-17-7175-2017, 2017.

Cong, Z., Kang, S., Gao, S., Zhang, Y., Li, Q., and Kawamura, K.: Historical trends of atmospheric black carbon on Tibetan Plateau as reconstructed from a 150-year lake sediment record, Environ. Sci. Technol., 47, 2579–2586, 2013.

Cong, Z., Kang, S., Kawamura, K., Liu, B., Wan, X., Wang, Z., Gao, S., and Fu, P.: Carbonaceous aerosols on the south edge of the Tibetan Plateau: concentrations, seasonality and sources, Atmos. Chem. Phys., 15, 1573–1584, https://doi.org/10.5194/acp-15-1573-2015, 2015.

Deaton, B. C. and Balsam, W. L.: Visible spectroscopy–a rapid method for determining hematite and goethite concentration in geological materials, J. Sediment. Res., 61, 628–632, 1991.

Di Mauro, B., Baccolo, G., Garzonio, R., Giardino, C., Massabò, D., Piazzalunga, A., Rossini, M., and Colombo, R.: Impact of impurities and cryoconite on the optical properties of the Morteratsch Glacier (Swiss Alps), The Cryosphere, 11, 2393–2409, https://doi.org/10.5194/tc-11-2393-2017, 2017.

Doherty, S. J., Warren, S. G., Grenfell, T. C., Clarke, A. D., and Brandt, R. E.: Light-absorbing impurities in Arctic snow, Atmos. Chem. Phys., 10, 11647–11680, https://doi.org/10.5194/acp-10-11647-2010, 2010.

Dong, Z., Qin, D., Chen, J., Qin, X., Ren, J., Cui, X., Du, Z., and Kang, S.: Physicochemical impacts of dust particles on alpine glacier meltwater at the Laohugou Glacier basin in western Qilian Mountains, China, Sci. Total Environ., 493, 930–942, 2014.

Dong, Z., Kang, S., Qin, D., Li, Y., Wang, X., Ren, J., Li, X., Yang, J., and Qin, X.: Provenance of cryoconite deposited on the glaciers of the Tibetan Plateau: New insights from Nd-Sr isotopic composition and size distribution, J. Geophys. Res.-Atmos., 121, 7371–7382, 2016.

Flanner, M. G. and Zender, C. S.: Linking snowpack microphysics and albedo evolution, J. Geophys. Res., 111, D12208, https://doi.org/10.1029/2005JD006834, 2006.

Formenti, P., Caquineau, S., Chevaillier, S., Klaver, A., Desboeufs, K., Rajot, J.-L., Belin, S., and Briois, V.: Dominance of goethite over hematite in iron oxides of mineral dust from Western Africa: Quantitative partitioning by X-ray absorption spectroscopy, J. Geophys. Res.-Atmos., 119, 12740–12754, https://doi.org/10.1002/2014JD021668, 2014.

Fru, E. C., Piccinelli, P., and Fortin, D.: Insights into the Global Microbial Community Structure Associated with Iron Oxyhydroxide Minerals Deposited in the Aerobic Biogeosphere, Geomicrobiol. J., 29, 587–610, 2012.

Gao, Y., Kaufman, Y., Tanre, D., Kolber, D., and Falkowski, P.: Seasonal distributions of aeolian iron fluxes to the global ocean, Geophys. Res. Lett., 28, 29–32, 2001.

Gomes, L. and Gillette, D. A.: A comparison of characteristics of aerosol from dust storms in central Asia with soil-derived dust from other regions, Atmos. Environ. A Gen., 27, 2539–2544, 1993.

Grenfell, T. C., Doherty, S. J., Clarke, A. D., and Warren, S. G.: Light absorption from particulate impurities in snow and ice determined by spectrophotometric analysis of filters, Appl. Optics, 50, 2037–2048, 2011.

Han, Y., Cao, J., An, Z., Chow, J. C., Watson, J. G., Jin, Z., Fung, K., and Liu, S.: Evaluation of the thermal/optical reflectance method for quantification of elemental carbon in sediments, Chemosphere, 69, 526–533, 2007.

Han, Y. M., Cao, J. J., Yan, B. Z., Kenna, T. C., Jin, Z. D., Cheng, Y., Chow, J. C., and An, Z. S.: Comparison of Elemental Carbon in Lake Sediments Measured by Three Different Methods and 150-Year Pollution History in Eastern China, Environ. Sci. Technol., 45, 5287–5293, 2011.

Hawkings, J. R., Benning, L. G., Raiswell, R., Kaulich, B., Araki, T., Abyaneh, M., Stockdale, A., Koch-Müller, M., Wadham, J. L., and Tranter, M.: Biolabile ferrous iron bearing nanoparticles in glacial sediments, Earth Planet. Sc. Lett., 493, 92–101, 2018.

IPCC: Climate change 2013: the physical science basis: Working Group I contribution to the Fifth assessment report of the Intergovernmental Panel on Climate Change, Cambridge University Press, Cambridge, UK, 2014.

Ji, J. F., Balsam, W., Chen, J., and Liu, L. W.: Rapid and quantitative measurement of hematite and goethite in the Chinese loess-paleosol sequence by diffuse reflectance spectroscopy, Clays Clay Miner., 50, 208–216, 2002.

Kaspari, S., Painter, T. H., Gysel, M., Skiles, S. M., and Schwikowski, M.: Seasonal and elevational variations of black carbon and dust in snow and ice in the Solu-Khumbu, Nepal and estimated radiative forcings, Atmos. Chem. Phys., 14, 8089–8103, https://doi.org/10.5194/acp-14-8089-2014, 2014.

Kaspari, S., Skiles, S. M., Delaney, I., Dixon, D., and Painter, T. H.: Accelerated glacier melt on Snow Dome, Mount Olympus, Washington, USA, due to deposition of black carbon and mineral dust from wildfire, J. Geophys. Res.-Atmos., 120, 2793–2807, 2015.

Kaspari, S. D., Schwikowski, M., Gysel, M., Flanner, M. G., Kang, S., Hou, S., and Mayewski, P. A.: Recent increase in black carbon concentrations from a Mt. Everest ice core spanning 1860–2000 AD, Geophys. Res. Lett., 38, L04703, https://doi.org/10.1029/2010GL046096, 2011.

Lafon, S., Rajot, J. L., Alfaro, S. C., and Gaudichet, A.: Quantification of iron oxides in desert aerosol, Atmos. Environ., 38, 1211–1218, 2004.

Lafon, S., Sokolik, I. N., Rajot, J. L., Caquineau, S., and Gaudichet, A.: Characterization of iron oxides in mineral dust aerosols: Implications for light absorption, J. Geophys. Res., 111, D21207, https://doi.org/10.1029/2005JD007016, 2006.

Lu, W., Zhao, W., Balsam, W., Lu, H., Liu, P., Lu, Z., and Ji, J.: Iron Mineralogy and Speciation in Clay-Sized Fractions of Chinese Desert Sediments, J. Geophys. Res.-Atmos., 122, 13458–13471, https://doi.org/10.1002/2017JD027733, 2017.

Mehra, O. P. and Jackson, M. L.: Iron oxide removal from soils and clays by a dithionite–citrate system buffered with sodium bicarbonate, Clay. Clay Miner., 7, 317–327, 1958.

Moosmüller, H., Engelbrecht, J. P., Skiba, M., Frey, G., Chakrabarty, R. K., and Arnott, W. P.: Single scattering albedo of fine mineral dust aerosols controlled by iron concentration, J. Geophys. Res., 117, D11210, https://doi.org/10.1029/2011JD016909, 2012.

Niu, H., He, Y., Zhu, G., Xin, H., Du, J., Pu, T., Lu, X., and Zhao, G.: Environmental implications of the snow chemistry from Mt. Yulong, southeastern Tibetan Plateau, Quatern. Int., 313–314, 168–178, 2013.

Painter, T. H., Deems, J. S., Belnap, J., Hamlet, A. F., Landry, C. C., and Udall, B.: Response of Colorado River runoff to dust

radiative forcing in snow, P. Natl. Acad. Sci. USA, 107, 17125–17130, 2010.

Pu, W., Wang, X., Wei, H., Zhou, Y., Shi, J., Hu, Z., Jin, H., and Chen, Q.: Properties of black carbon and other insoluble light-absorbing particles in seasonal snow of northwestern China, The Cryosphere, 11, 1213–1233, https://doi.org/10.5194/tc-11-1213-2017, 2017.

Qian, Y., Yasunari, T. J., Doherty, S. J., Flanner, M. G., Lau, W. K. M., Ming, J., Wang, H., Wang, M., Warren, S. G., and Zhang, R.: Light-absorbing Particles in Snow and Ice: Measurement and Modeling of Climatic and Hydrological impact, Adv. Atmos. Sci., 32, 64–91, 2015.

Reynolds, R. L., Goldstein, H. L., Moskowitz, B. M., Bryant, A. C., Skiles, S. M., Kokaly, R. F., Flagg, C. B., Yauk, K., Berquo, T., Breit, G., Ketterer, M., Fernandez, D., Miller, M. E., and Painter, T. H.: Composition of dust deposited to snow cover in the Wasatch Range (Utah, USA): Controls on radiative properties of snow cover and comparison to some dust-source sediments, Aeolian Res., 15, 73–90, 2014.

Schlitzer, R.: Ocean Data View, available at: odv.awi.de (last access: 2 Ocotber 2018), 2017.

Schwertmann, U.: Transformation of Hematite to Goethite in Soils, Nature, 232, 624–625, 1971.

Shahgedanova, M., Kutuzov, S., White, K. H., and Nosenko, G.: Using the significant dust deposition event on the glaciers of Mt. Elbrus, Caucasus Mountains, Russia on 5 May 2009 to develop a method for dating and "provenancing" of desert dust events recorded in snow pack, Atmos. Chem. Phys., 13, 1797–1808, https://doi.org/10.5194/acp-13-1797-2013, 2013.

Shen, Z. X., Cao, J. J., Zhang, X. Y., Arimoto, R., Ji, J. F., Balsam, W. L., Wang, Y. Q., Zhang, R. J., and Li, X. X.: Spectroscopic analysis of iron-oxide minerals in aerosol particles from northern China, Science of The Total Environment, 367, 899-907, 2006.

Shi, Z., Krom, M. D., Jickells, T. D., Bonneville, S., Carslaw, K. S., Mihalopoulos, N., Baker, A. R., and Benning, L. G.: Impacts on iron solubility in the mineral dust by processes in the source region and the atmosphere: A review, Aeolian Res., 5, 21–42, 2012.

Sokolik, I. N. and Toon, O. B.: Incorporation of mineralogical composition into models of the radiative properties of mineral aerosol from UV to IR wavelengths, J. Geophys. Res., 104, 9423–9444, https://doi.org/10.1029/1998JD200048, 1999.

Takeuchi, N.: Optical characteristics of cryoconite (surface dust) on glaciers: the relationship between light absorbency and the property of organic matter contained in the cryoconite Ann. Glaciol., 34, 409–414, 2002.

Taylor, S. R. and McLennan, S. M.: The geochemical evolution of the continental crust, Rev. Geophys., 33, 241–265, 1995.

Tian, L., Masson-Delmotte, V., Stievenard, M., Yao, T., and Jouzel, J.: Tibetan Plateau summer monsoon northward extent revealed by measurements of water stable isotopes, J. Geophys. Res.-Atmos., 106, 28081–28088, 2001.

Utry, N., Ajtai, T., Pintér, M., Tombácz, E., Illés, E., Bozóki, Z., and Szabó, G.: Mass-specific optical absorption coefficients and imaginary part of the complex refractive indices of mineral dust components measured by a multi-wavelength photoacoustic spectrometer, Atmos. Meas. Tech., 8, 401–410, https://doi.org/10.5194/amt-8-401-2015, 2015.

Wang, M., Xu, B., Kaspari, S. D., Gleixner, G., Schwab, V. F., Zhao, H., Wang, H., and Yao, P.: Century-long record of black carbon in an ice core from the Eastern Pamirs: Estimated contributions from biomass burning, Atmos. Environ., 115, 79–88, 2015.

Wang, P., Li, Z., Li, H., Wang, W., and Yao, H.: Comparison of glaciological and geodetic mass balance at Urumqi Glacier No. 1, Tian Shan, Central Asia, Global Planet. Change, 114, 14–22, 2014.

Wang, X., Doherty, S. J., and Huang, J.: Black carbon and other light-absorbing impurities in snow across Northern China, J. Geophys. Res.-Atmos., 118, 1471–1492, 2013.

Warren, S. G. and Wiscombe, W. J.: Dirty snow after nuclear war, Nature, 313, 467–470, 1985.

Wu, G., Xu, B., Zhang, C., Gao, S., and Yao, T.: Geochemistry of dust aerosol over the Eastern Pamirs, Geochim. Cosmochim. Ac., 73, 977–989, 2009.

Wu, G., Zhang, C., Li, Z., Zhang, X., and Gao, S.: Iron content and solubility in dust from high-alpine snow along a north-south transect of High Asia, Tellus B, 64, 17735, https://doi.org/10.3402/tellusb.v64i0.17735, 2012.

Wu, G.-M., Cong, Z.-Y., Kang, S.-C., Kawamura, K., Fu, P.-Q., Zhang, Y.-L., Wan, X., Gao, S.-P., and Liu, B.: Brown carbon in the cryosphere: Current knowledge and perspective, Advances in Climate Change Research, 7, 82–89, 2016.

Yang, W., Guo, X., Yao, T., Zhu, M., and Wang, Y.: Recent accelerating mass loss of southeast Tibetan glaciers and the relationship with changes in macroscale atmospheric circulations, Clim. Dynam., 47, 805–815, https://doi.org/10.1007/s00382-015-2872-y, 2016.

Yasunari, T. J., Bonasoni, P., Laj, P., Fujita, K., Vuillermoz, E., Marinoni, A., Cristofanelli, P., Duchi, R., Tartari, G., and Lau, K.-M.: Estimated impact of black carbon deposition during pre-monsoon season from Nepal Climate Observatory – Pyramid data and snow albedo changes over Himalayan glaciers, Atmos. Chem. Phys., 10, 6603–6615, https://doi.org/10.5194/acp-10-6603-2010, 2010.

Zhang, X. L., Wu, G. J., Zhang, C. L., Xu, T. L., and Zhou, Q. Q.: What is the real role of iron oxides in the optical properties of dust aerosols?, Atmos. Chem. Phys., 15, 12159–12177, https://doi.org/10.5194/acp-15-12159-2015, 2015.

Zhou, Y., Wang, X., Wu, X., Cong, Z., Wu, G., and Ji, M.: Quantifying Light Absorption of Iron Oxides and Carbonaceous Aerosol in Seasonal Snow across Northern China, Atmosphere, 8, 63, https://doi.org/10.3390/atmos8040063, 2017.